Spatial-temporal variation of satellite-based gross primary production estimation in wheat-maize rotation area during 2000–2015

Wenquan Xie , Huini Wang , Hong Chi , Haishan Dang , Duan Huang , Hui Li , Guoqing Cai & Xiangming Xiao

GEOCARTO INTERNATIONAL
https://doi.org/10.1080/10106049.2020.1822928

Spatial-temporal variation of satellite-based gross primary production estimation in wheat-maize rotation area during 2000–2015

Wenquan Xie[a,b], Huini Wang[c], Hong Chi[d,e], Haishan Dang[f], Duan Huang[g], Hui Li[a], Guoqing Cai[a] and Xiangming Xiao[e]

[a]School of Geographic Sciences, Xinyang Normal University, Xinyang, China; [b]Key Laboratory for Synergistic Prevention of Water and Soil Environmental Pollution, Xinyang Normal University, Xinyang, China; [c]School of Civil Engineering and Architecture, Wuhan Institute of Technology (Wuchang Campus), Wuhan, China; [d]Key laboratory for Environment and Disaster Monitoring and Evaluation of Hubei province, Innovation Academy for Precision Measurement Science and Technology, Chinese Academy of Sciences, Wuhan, China; [e]Department of Microbiology and Plant Biology, Center for Spatial Analysis, University of Oklahoma, Norman, OK, USA; [f]Key Laboratory of Aquatic Botany and Watershed Ecology, Wuhan Botanical Garden, Chinese Academy of Sciences, Wuhan, China; [g]Faculty of Geomatics, East China University of Technology, Nanchang, China

ABSTRACT

North China Plain is the largest agricultural production center in China and wheat-maize rotation is a widespread cultivation practice in this area. As gross primary production (GPP) is a proxy of land productivity, research on its spatial-temporal dynamics helps understand the variation of grain production in wheat-maize rotation. Here, Moderate Resolution Imaging Spectroradiometer (MODIS) data and ground observation data were combined to drive Vegetation Photosynthesis Model (VPM) in GPP estimation over wheat-maize rotation area during 2000–2015. Annual GPP has increased by 540.95 g C m^{-2} $year^{-1}$ from 2000 to 2015, while total annual GPP has grown $\sim$150% than that of 2000. Moreover, annual GPP showed an increasing trend in the consecutively wheat-maize rotation area between 2000 and 2015. A strong linear relationship between GPP estimates and grain production demonstrated the potential of using VPM model to evaluate grain production in wheat-maize rotation area of Henan province, China.

ARTICLE HISTORY
Received 2 June 2020
Accepted 17 August 2020

KEYWORDS
Gross primary production; grain production; wheat-maize rotation; VPM model; MODIS

1. Introduction

Food security is under constant pressure from increasing the human population and environmental changes, which is a great challenge for sustainable development (Mc Carthy et al. 2018). Timely and accurate estimation of grain production benefits evidence-informed policy and decisions on adequately managing and distributing the food supply that reduces food security threats. As the gross primary production (GPP) is used to

CONTACT Huini Wang wanghuini@wit.edu.cn; Hong Chi chihong@whigg.ac.cn
Supplemental data for this article can be accessed at https://doi.org/10.1080/10106049.2020.1822928.

quantify the total amount of energy or biomass produced through vegetation photosynthesis in a given length of time (Spielmann et al. 2019), productivity in agricultural ecosystems is key to understand their role of capturing energy (carbon) in the form of food products, e.g. agricultural yield. GPP of agricultural ecosystems, a proxy of land productivity (Ma et al. 2020), is the amount of total carbon assimilated by the planted crops and the driver of useful biomass production.

Obtaining regional information of grain production through surveys is relatively popular, but they are of fairly high cost and still have associated uncertainties (Gallego et al. 2010). Alternatively, crop production or crops GPP estimated from remotely-sensed data has been widely used among different management practices. GPP of globally widespread crops, such as wheat, maize, rice, soybeans, and rapeseed, have been investigated extensively in many studies (Kalfas et al. 2011; Sanchez et al. 2015; Wagle et al. 2015; Xin F et al. 2020). Eddy covariance flux towers indirectly derive GPP as the difference between net ecosystem exchange (NEE) and ecosystem respiration during daylight. Although the increasing number of covariance flux towers in various biomes around the world has provided a perception of GPP geographical variability (Baldocchi et al. 2001), regional-scale GPP estimation of cropland and its dynamic changes in time and space are urgently required with the growth of food demand.

Light use efficiency (LUE) models are considered a robust tool as it can describe GPP spatial and temporal variation among the available satellite-based estimation methods (Sanchez et al. 2015). These models were built on the assumption that GPP of terrestrial ecosystem is directly related to the absorbed photosynthetically active radiation (PAR) through LUE (Monteith 1977). That is to say, GPP was estimated from these models as a product of absorbed photosynthetically active radiation (APAR) and LUE (ε_g) ($GPP = APAR \times \varepsilon_g$). An earlier study of LUE models employed the fraction of photosynthetically active radiation (PAR) absorbed by the vegetation canopy ($FPAR_{canopy}$) to estimate $APAR_{canopy}$ ($APAR_{canopy} = (PAR) \times (FPAR)_{canopy}$), and $FPAR_{canopy}$ being approximated using vegetation indices (Potter et al. 1993; Zhao et al. 2005), which could be derived from remotely sensed optical imagery. Remote sensing of earth observation provided consistent fine-scale measurements and facilitate the monitoring process of the ecosystem exchange at larger scales (DeFries 2008). As one of widely used LUE model, Vegetation Photosynthesis Model (VPM) advanced estimation of the amount of PAR absorbed by photosynthetically active vegetation (PAV, e.g. mostly green leaves) of vegetation canopy for photosynthesis and quantification of light use efficiency of vegetation (Xiao, Zhang, et al. 2004). The satellite-based model has been successfully employed to estimate GPP by use of flux measurements from a variety of CO_2 flux tower sites, including forests (Xiao, Hollinger, et al. 2004; Xiao, Zhang, et al. 2004), savannas (Jin et al. 2013), grassland (Wagle et al. 2014), crops (Xin et al. 2017; Ma et al. 2020), and wetland (Kang et al. 2018).

Based on the concept of Monteith (1977), LUE (ε_g) depends on vegetation type and suboptimal climate conditions. Previous relevant studies (Lobell et al. 2002; Bradford et al. 2005) indicated that differences among crop types in carboxylation biochemistry (especially, the C_3 and C_4 pathways) suggest associated differences in production efficiency, which is linked to photosynthetic potential. Because C_4 plants have a more efficient photosynthetic capacity than C_3 plants, the assignment of one fixed ε_g value across an entire year is problematic (Yan et al. 2009). As we know, winter-wheat and summer-maize double–cropping rotation system is one of extensive C_3–C_4 crop rotation systems in global cropland, especially in the North China Plain (NCP) (Yan et al. 2009), which is the largest and most important agricultural region in China (Wang et al. 2015; Bao et al. 2019). Henan province, located in the NCP, is one of the major grain-producing provinces, and produced more than 28% and 9% of the national winter-wheat production and summer-maize production in 2018, respectively (http://data.stats.gov.cn/). Although some signs of progress on GPP estimation of wheat and maize crop rotation in the NCP were achieved in recent years (Yan et al. 2009; Wang et al. 2015; Zhang, Lei, et al. 2020), these studies were based on CO_2 eddy flux tower sites and the impact of double cropping on the regional GPP estimation caused by changes in land surface conditions remains unknown. Meanwhile, crops growing seasons and fallow periods were varied within crop rotation pattern as affected by crop management practices in Henan province. Despite these time-gap variations were considered at site-scale, it still remains a challenge to monitor GPP dynamics changes of croplands temporally and spatially at the regional scale, especially for the widespread wheat-maize rotation area (WMRA) in a long time series.

The aim of this study was to better understand the spatial-temporal variation of satellite-based GPP in WMRA (with consecutively cropping practice and non-consecutively cropping practice) of Henan province during 2000–2015. First, WMRA was obtained by overlaying wheat planting area and maize planting area from a basic dataset of crop planting area, and compared with planting area from agricultural statistical reports. Second, annual GPP was estimated from the VPM model, and evaluated by the grain production from the state statistical report. Third, interannual trend in GPP was analyzed in the consecutively WMRA and non-consecutively WMRA. Based on the analysis of relationships between GPP and the number of years as (consecutively) wheat-maize rotation in temporal and spatial, we try to answer whether grain production could be promoted by increase the number of years as (consecutively) wheat-maize rotation and where is appropriate for high-yield wheat-maize rotation.

2. Materials and methods

2.1. Study area

Henan is a landlocked province, which is located in the central region of China (Figure 1). Henan has a diverse landscape with floodplains in the east and mountains in the west. Most of Henan province has a temperate climate that belongs to the continental monsoon climate transition from the north subtropical zone to the warm temperate zone. It has a distinct seasonal climate characterized by hot and humid summers and generally cold and windy in winters. The average temperature of the province is between 12 and 16 °C, which meets the need of one-year two-crops rotation practices (Zhu et al. 2020). The grain cropped area is about 10.9 million ha in 2018, accounting for nearly ⅔ of the Henan province area (http://data.stats.gov.cn/). According to the historical meteorological data compiled by the China Meteorological Administration (CMA), the study area was divided into four agro-climatic zones (ACZs): that are Nanyang basin zone (ACZ 1), Huang-Huai floodplains zone (ACZ 2), western mountainous zone (ACZ 3), and Hilly-plain transition zone (ACZ 4). In addition, 18 municipal districts of Henan province were shown in Figure S1.

2.2. Materials

2.2.1. Satellite imagery and vegetation indices

The MODIS sensor onboard the NASA Terra satellite was launched in December 1999. In the study, the 8-day composite land surface reflectance product (MOD09A1) at a 500-m spatial resolution from the USGS's Land Processes Distributed Active Archive Center (LPDAAC, https://lpdaac.usgs.gov/) was downloaded. Geometrical and atmospherically

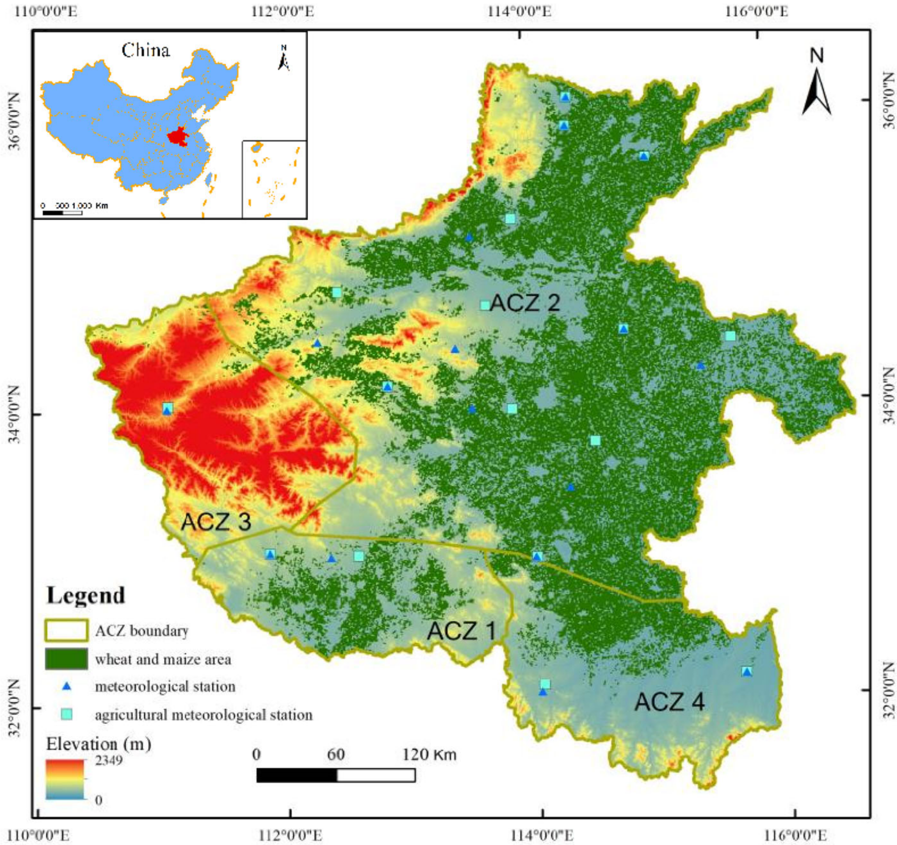

Figure 1. Introduction of study area (wheat and maize area was showed in 2015).

corrections and cloud contamination removal have already been processed in the MOD09A1 product (Huete et al. 2002; Justice et al. 2002). A total of 728 images from 18 February 2000 to 31 December 2018 were used to estimate vegetation indices for GPP estimation (Because of the sensor calibration, no observations were acquired on DOY (day of year) 169 and 177 in 2001). Based on the geo-location information of Henan province, the time–series images of land surface reflectance and quality flags in the study period were extracted from MODIS tiled grid data (h27v05). The vegetation indices were calculated by using 8-day composite surface reflectance data from the blue (459–479 nm), red (620–670 nm), near-infrared (841–875 nm) and shortwave infrared (SWIR, 1628–1652 nm) bands (Equation (1)–(2)): (1) Enhanced Vegetation Index (EVI; Huete et al. 1997), and (2) Land Surface Water Index (LSWI; Xiao et al. 2002).

$$\mathrm{EVI} = \frac{2.5 \times (\rho_{\mathrm{NIR}} - \rho_{\mathrm{Red}})}{\rho_{\mathrm{NIR}} + 6 \times \rho_{\mathrm{Red}} - 7.5 \times \rho_{\mathrm{Blue}} + 1} \tag{1}$$

$$\mathrm{LSWI} = \frac{\rho_{\mathrm{NIR}} - \rho_{\mathrm{SWIR}}}{\rho_{\mathrm{NIR}} + \rho_{\mathrm{SWIR}}} \tag{2}$$

Although MOD09A1 product contain the best observations within the 8-day composite periods to eliminate the effects of atmosphere and clouds, invalid or noisy observations affected by external factors in the product should be smoothed. These abnormal observations were detected according to the quality assurance layer in the dataset. Poor quality data were substituted with the linear interpolation of its predecessor and successor as reported in earlier studies (Xiao, Zhang, et al. 2004; Yan et al. 2009), and smoothed using a Savitzky-Golay filter (Savitzky and Golay 1964), which can be used to reduce the random noise and widely used for the reconstruction of time–series of remotely-sensed vegetation indices (Zhang et al. 2017; Silva et al. 2019).

2.2.2. Wheat and maize planting area data

Annual wheat and maize planting areas data at a spatial resolution of 1 km from 2000 to 2015 was used in this study (Luo et al. 2020). The cropland area of the product was derived from the 1 km grid of the Chinese National Land Cover Dataset (NLCD) provided by the Data Center for Resources and Environmental Sciences, Chinese Academy of Sciences (http://www.resdc.cn/Default.aspx; Liu et al. 2014). Compared with cropland area data published by National Bureau of Statistics of China, the coefficient of determination between the statistical planting area data and NLCD-based planting area data is greater than 0.95 (0.99 for wheat planting area, maize planting area, and wheat and maize planting area, respectively, Figure S2). The good accuracy of the cropland area data has been showed in a recent study (Zhang, Zhang, et al. 2020).

2.2.3. Ground observation data

Ground observation data mainly contains crop phenology information and meteorological data. Crop phenology is an important parameter in VPM model for GPP estimation at regional scale due to its significant variation over a large spatial range. The ground observation data includes the field records of crop growth and development status, such as the name of the crop, development stages with theirs date, the anomaly of the crop development stage, and the degree of the development stage, and so on (Luo et al. 2020). The start of the season (SOS) and the end of the season (EOS) of wheat and maize from 2000 to 2013 were collected from agricultural meteorological stations (AMSs) of CMA (https://data.cma.cn/). In Total, there were 17 AMSs across the main cropland area in Henan province were obtained for identification of the crop phenology in four ACZs. Due to lack of crop phenology information in 2014 and 2015, the mean SOS and EOS of crops from 2011 to 2013 were assigned as SOS and EOS of 2014, and the averaged SOS and EOS of crops from 2012 to 2014 were assigned as SOS and EOS of 2015 (the result is showed in the Excel file of the Supplementary Materials).

The meteorological data used to drive the VPM model consisted of daily mean temperature and daily total sunshine duration. These data were derived from 25 meteorological stations in Henan province from 2000 to 2015. The total sunshine duration was used to calculate total solar radiation based on ÅngstrÖm–Prescott (Å–P) method (Angstrom 1924). The Å–P method for solar radiation estimation has been adopted as the standard procedure in evapotranspiration by FAO in 1998 (Allen et al. 1998). The empirical coefficients used Å–P method were extracted from previous researches (Zuo et al. 1963). Then, PAR (photosynthetically active radiation) was estimated to be 45% of the total solar radiation (Meek et al. 1984). After processing the site observation data, the thin plate spline smoothing algorithms was applied to interpolate 8-day mean temperature (with ASTER GDEM (Advanced Spaceborne Thermal Emission and Reflection Radiometer Global Digital Elevation Model) as a covariate, http://www.gscloud.cn) and 8-day PAR to produce meteorological raster images with a spatial resolution of 500 m in ANUSPLIN (Hutchinson 2002) to match the pixel size of MODIS imagery.

2.2.4. Agricultural statistical data during 2000–2015

The datasets of wheat and maize plating area, and theirs grain production in Henan province in 2000–2015 were obtained from the agricultural statistical reports (http://data.stats.gov.cn/). Previous studies indicated that carbon constitutes about 45% of crop grain production (Lobell et al. 2003). Therefore, carbon content of grain production (g C year^{-1}) as 0.45 of the grain production (ton year^{-1}) was calculated in the study, which allow us to evaluate the relationship between annual GPP and annual grain production of wheat and maize, respectively.

2.3. Methods

2.3.1. GPP estimation from VPM model

Based on the concept that vegetation canopy is composed of photosynthetically active vegetation (mostly chlorophyll (chl)) and non-photosynthetic vegetation (NPV) as well as only the chlorophyll component of the canopy is used for photosynthesis, the VPM model was developed to estimate gross primary production over the photosynthetically active period of vegetation as the product of amount of photosynthetically active radiation (PAR) absorbed by chlorophyll ($APAR_{chl} = (FPAR)_{chl} \times (PAR)$) and light use efficiency (Xiao, Hollinger, et al. 2004). The VPM is described as the following Equation (3):

$$GPP = \varepsilon_g \times (FPAR)_{chl} \times (PAR) \tag{3}$$

where PAR is the photosynthetically active radiation (μmol photosynthetic photon flux density, PPFD), and ε_g is the light use efficiency for GPP (μmol CO_2 μmol PPFD^{-1} or g C mol PPFD^{-1}). $(FPAR)_{chl}$ within the photosynthetically active period of vegetation is estimated as a linear function of EVI (Equation (4)), and the coefficient α is set to be 1.0 (Xiao, Hollinger, et al. 2004):

$$FPAR_{chl} = \alpha \times EVI \tag{4}$$

light use efficiency is affected by temperature, water, which can be expressed in the following Equation (5):

$$\varepsilon_g = \varepsilon_0 \times T_{scalar} \times W_{scalar} \tag{5}$$

where ε_0 is the apparent quantum yield or maximum light use efficiency. Ecosystem-level ε_0 values can be acquired from analysis of net ecosystem exchange (NEE) of CO_2 and incident PAR (μmol m^{-2} s^{-1}) at CO_2 eddy flux tower sites, either by using the hyperbolic light response function (Goulden et al. 1997; Falge et al. 2001) or from the literature. In this study, the ε_0 values were set to be 0.76 g C mol PPFD^{-1} of winter wheat and 0.92 g C mol PPFD^{-1} of maize based on analyses of half-hourly NEE and incident PAR data during 2003–2004 at the Yucheng site, China, because this site is located in the NCP and share the same cropping practices with Henan province (Yan et al. 2009). T_{scalar} and W_{scalar} are the scalars for the effects of temperature and water on light use efficiency of vegetation, respectively. The effect of temperature on photosynthesis (T_{scalar}) is estimated from the equation developed for the Terrestrial Ecosystem Model (Raich et al. 1991; Equation (6)):

$$T_{scalar} = \frac{(T - T_{min}) \times (T - T_{max})}{(T - T_{min}) \times (T - T_{max}) - (T - T_{opt})^2} \tag{6}$$

where T_{min}, T_{max} and T_{opt} are minimum, maximum and optimal temperature for photosynthetic activities, respectively. In this study, T_{min} and T_{max} were set to -3 and 42 °C for winter wheat, and 0 and 45 °C for maize (Chen et al. 2014). The optimum temperature (T_{opt}) is defined as the long-term mean temperature for the growing season based on the concept that plants grow efficiently at the prevailing temperature (Sellers et al. 1992), and were set 16 °C for winter wheat and 23 °C for maize (Chen et al. 2014). If air temperature falls below T_{min}, T_{scalar} is set to be zero. The effect of water on plant photosynthesis (W_{scalar}) was estimated from satellite-derived Land Surface Water Index in Equation (7):

$$\mathrm{W_{scalar}} = \frac{1 + \mathrm{LSWI}}{1 + (\mathrm{LSWI})_{\max}} \tag{7}$$

where $(\mathrm{LSWI})_{max}$ is the maximum LSWI during the growing season of crops for each pixel based on the analysis of LSWI seasonal dynamics derived from MODIS data. The maximum of LSWI value within the growing season of crops was used as an approximation of $(\mathrm{LSWI})_{max}$ (Xiao, Hollinger, et al. 2004).

2.3.2. WMRA statistics

Based on the data products of annual wheat and maize planting area during 2000–2015 (Luo et al. 2020), we used boundary vector data of Henan province as well as its municipalities to extract theirs cropland area of wheat and maize. In order to evaluate the sustainable development potential of cropland in C_3-C_4 rotation areas, two statistical indicators of WMRAs were extracted from the crop planting area data between 2000 and 2015. The first one was the number of years as wheat-maize rotation area (NYWM). Wheat pixels and maize pixels were overlapped to extract WMRA from 2000 to 2015. The WMRA was counted at provincial scale and municipal scale to examine the theirs trends during 2000–2015. A frequency (NYWM) map was then generated by overlaying WMRA maps during the period 2000–2015. The second indicator was the number of years as consecutively wheat-maize rotation area (NYCWM). There were two indicators of NYCWM, one was annual consecutively wheat-maize rotation area (CWMRA). We counted the pixels in consecutively wheat-maize rotation from 2 to 16 years, that meant CWMRA between 2000–2001, 2000–2002, 2000–2003, …, 2000–2015 were recorded. The other was 16-year consecutively wheat-maize rotation area (16 y-CWMRA). We overlapped WMRA during 2000–2015, and extracted the area that wheat-maize rotation cropping every year over the 16 years.

2.3.3. GPP estimation of WMRA

As photosynthetic process is closely related to the length of crop growing season (LOS), pixel-level GPP of Henan province was estimated from VPM model in LOS of wheat and maize. LOS of wheat and maize was estimated from SOS and EOS data derived from the ground observation at AMSs in four ACZs. Due to the model-driven data are 8-day composite EVI data and meteorological data, the positions of the first day of SOS and the last day of EOS in a given 8-day period were considered to determine how many 8-day data used in GPP estimation. In views of the lower GPP at the beginning of SOS and relative higher GPP at the ending of EOS, the processing of crop GPP estimation during SOS and EOS was based on the following three criteria:

1. if the first day of SOS is located in the first half of a given 8-day, GPP of the 8-day will be counted in the total GPP;
2. if the first day of SOS is located in the second half of a given 8-day, GPP of the 8-day will be dismissed;
3. no matter what's position of the last day of EOS in one 8-day, GPP of the 8-day will be counted.

Then, annual GPP of WMRA was summed up by four ACZs from 2000 to 2015. We used the simple linear regression model (GPP $= a \times$ Year $+ b$) to calculate the interannual trend of annual GPP during 2000–2015. Subsequently, to explore the overall relationship between GPP and cropping frequency, we calculated Pearson correlation coefficients (R) between number of years as wheat-maize rotation and corresponding mean annual GPP from 2000 to 2015.

2.3.4. Relationship between annual GPP and grain production of wheat and maize during 2000–2015

As wheat and maize grain production in statistical data were separately recorded, a simple linear regression model was used to assess the relationship between annual GPP and grain production (GP) of wheat and maize during 2000–2015, respectively. Due to the growing season of wheat spanning two calendar years, only 15-year comparisons were investigated in wheat crop, while 16-year comparisons were analyzed in maize crop. The linear regression model is expressed as a simple equation: $\mathrm{GP} = \mathrm{GPP} \times (\mathrm{HI})_{\mathrm{GPP}}$, where $(\mathrm{HI})_{\mathrm{GPP}}$ is Harvest Index (HI), defined as the ratio between grain production and GPP (Xin et al. 2020). It is different from the widely used HI that is defined as the ratio between grain production and aboveground biomass ($\mathrm{GP} = \mathrm{GPP} \times (\mathrm{HI})_{\mathrm{AGB}}$) or the ration between grain production and net primary production ($\mathrm{GP} = \mathrm{GPP} \times (\mathrm{HI})_{\mathrm{NPP}}$) (Lobell et al. 2002). That because this study focused on the GPP estimation and its dynamic change, the direct comparison of GPP and GP is more appropriate than the comparison of NPP and GP, or AGB and GP.

3. Results

3.1. Spatial-temporal variation of wheat and maize planting area as well as WMRA

The trends of wheat planting area and maize planting area of each municipality in Henan province are showed in Figures S3 and S4. Wheat planting area increased in 15 of 18 municipalities, while maize planting area increased in 17 of 18 municipalities during 2000–2015. Zhoukou municipality showed the greatest average annual growth rate both in wheat planting area and maize planting area with 17.95×10^3 ha year^{-1} and 11.23×10^3 ha year^{-1}, respectively. Figure S5 indicates the trend of WMRA of each municipality in Henan province during 2000–2015. Five municipalities demonstrated an increasing trend more than 10×10^3 ha year^{-1} (that were Anyang, Puyang, Xinxiang, Zhoukou and Zhumadian), and one municipality (that was sanmenxia) showed decreasing trend with 0.002×10^3 ha year^{-1}. In terms of entire province during the 16 years, WMRA illustrates a significant upward trend with average annual increase of $(111.73 \pm 6.36) \times 10^3$ ha year^{-1} ($p < 0.001$), growing by ~75% from 2000 (1945.18×10^3 ha) to 2015 (3384.80×10^3 ha) (Figure 2). The spatial distribution in Figure S6 shows the substantial growth of WMRA from north to south across Henan province from 2000 to 2015.

3.2. Spatial-temporal variation of GPP in WMRA

Spatial-temporal variation of GPP in WMRA is showed in Figure S7. A significant increasing trend of GPP in WMRA across the province from 2000 to 2015. Figure 2 indicates that there has been a gradual rise in the average annual increase rate of GPP in WMRA with 39.83 ± 6.96 g C m^{-2} per year ($p < 0.001$), experiencing ~50% growth from 2000 (1372.12 g C m^{-2}year^{-1}) to 2015 (1913.07 g C m^{-2}year^{-1}). Total annual GPP of

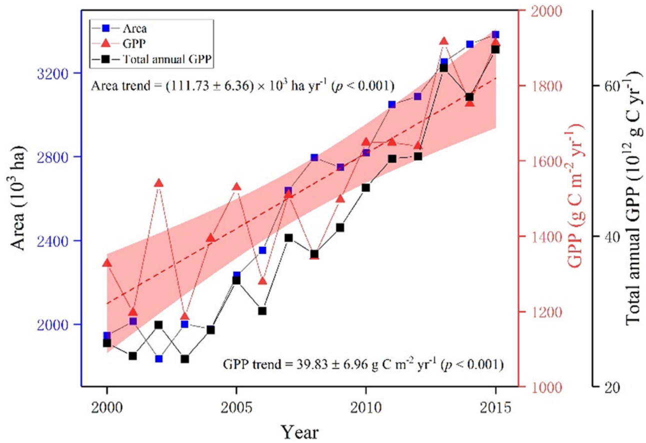

Figure 2. Trends of WMRA and corresponding GPP over the last 16 years (2000–2015). The blue squares connected by the solid lines represent the annual WMRA, the red triangles connected by the solid lines mean the annual GPP, and black squares connected by the solid lines stand for total annual GPP. Calculated trend (slope ± SE) based on ordinary least squares regression is given with its significance level. The significance was computed by using the non-parametric Mann-Kendall trend test and p-value are given in the figure where the dash lines represent the trend lines of GPP, and the shaded area represents the 95% confidence limit of the estimated slope in GPP.

WMRA has increased from 25.83×10^{12} g C year^{-1} in 2000 to 64.75×10^{12} g C year^{-1} in 2015, with an increase of 38.92×10^{12} g C year^{-1} (151%) and an average annual increase rate of 2.43×10^{12} g C year^{-1} over the 16-year period. The spatial distribution of CWMRA during 2000–2015 is illustrated in Figure S8. The annual CWMRA is significantly decreased from 2000 to 2006 (Table S1).

Figure 3 demonstrates spatial distribution of annual mean GPP of each pixel in WMRA from 2000 to 2015. The high values of GPP (>2000 g C m^{-2} year^{-1}) are located in the northern region and mid-east region of Henan province. The low values of GPP (<1000 g C m^{-2} year^{-1}) appear in the mid-western and southern region of Henan province.

The relationships between annual GPP and annual grain production of wheat and maize were examined in 2000–2015 (Figure 4). The slope values ($(HI)_{GPP}$) from simple linear regression models between annual grain production and annual GPP of wheat and maize are 0.31 and 0.33, respectively, in Henan province.

3.3. GPP of consecutively WMRA

To better understand the trend of GPP in the CWMRA, GPP of the consecutively cultivated area of wheat-maize rotation is showed in Figure 5. Top panel shows GPP (mean GPP in a given year when NYCWM during 1–16) upward trend along with the NYCWM. The simple linear model shows an average growth rate of 35.60 ± 6.55 g C m^{-2} year^{-1} ($p < 0.001$) ranging from 1370.65 g C m^{-2} year^{-1} in 2000 to 1924.68 g C m^{-2} year^{-1} in 2015. While, GPP of 16-year CWMRA also has demonstrated a significant increasing in fluctuation from 2000 (1394.74 g C m^{-2} year^{-1}) to 2015 (1924.68 g C m^{-2} year^{-1}) with 35.77 ± 6.57 g C m^{-2} per year ($p < 0.001$). The comparison between the top panel and bottom panel indicates high consistency in growing trend between mean annual GPP of the CWMRA and mean annual GPP of 16-year CWMRA.

In view of greater contingency in 2-year consecutively wheat-maize rotation, Figure 6 shows mean annual GPP in NYCWM rotation from 3 (NYCWM 2000–2002) to 16 (NYCWM 2000–2015). For a given year, variation of mean annual GPP is not significant

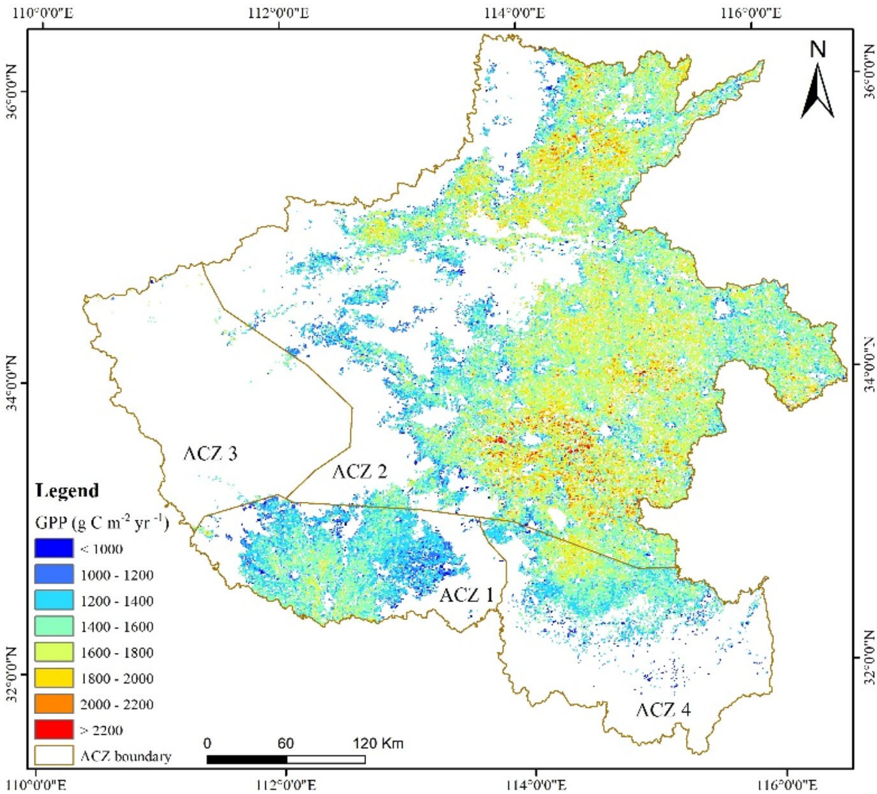

Figure 3. Average GPP in wheat-maize rotation area during 2000–2015 in Henan province, China.

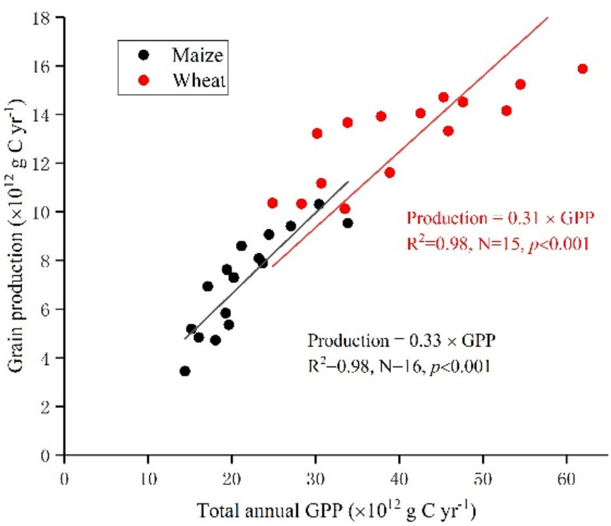

Figure 4. The relationship between total annual GPP and grain production for wheat and maize in Henan province, China.

when NYCWM varied between 3–16. While, when NYCMW > 8 (duration longer than 2000–2007), mean annual GPP shows a rise trend from 2008 to 2015 in a given NYCWM.

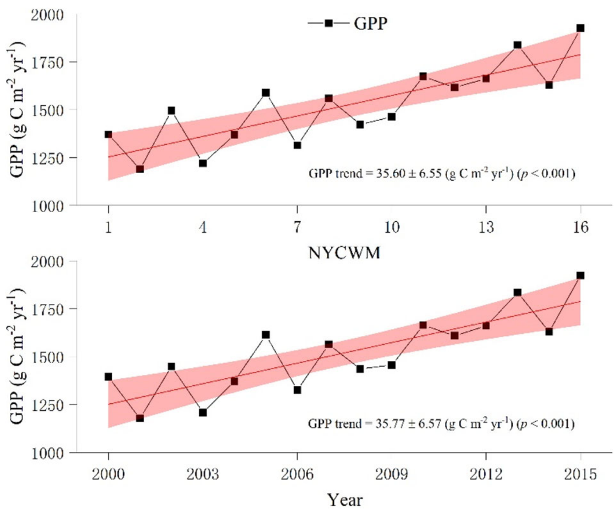

Figure 5. Trend of annual GPP in the consecutively wheat-maize rotation area and 16-year consecutively wheat-maize rotation area during 2000–2015 in Henan province, China. Estimated trend (slope ± SE) based on ordinary least squares regression is given with its significance level. The significance was computed by using the nonparametric Mann-Kendall trend test and p-value are given in the figure where the red solid lines represent the trend lines of GPP, and the shaded area represents the 95% confidence limit of the estimated slope in GPP (NYCWM means the number of years as consecutively wheat-maize rotation).

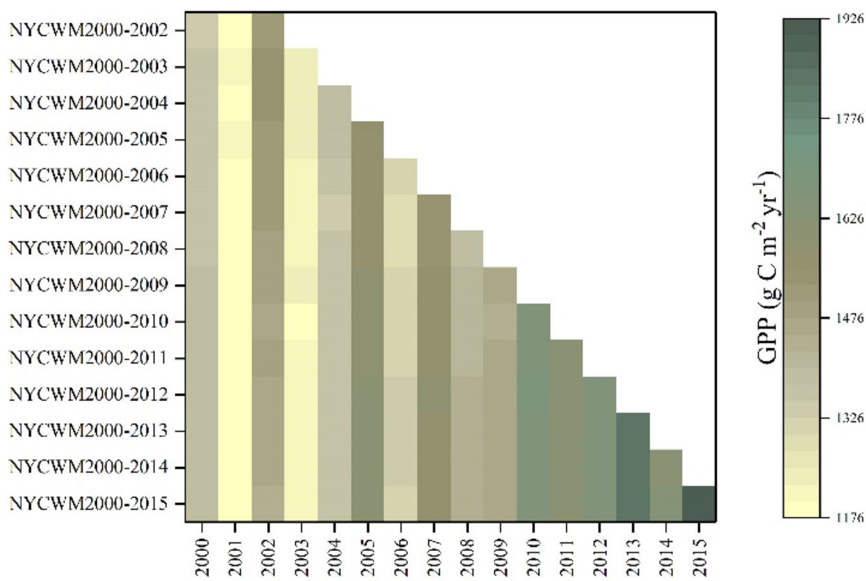

Figure 6. Heat map of mean annual GPP in different number of years as consecutively wheat-maize rotation area (NYCWM) during 2000–2015 in Henan province, China.

3.4. GPP of WMRA in various frequencies

Figure 7(a) indicates the NYWM during 2000–2015. Most of the high values of NYWM (NYWM > 10) are located in the north and mid-east region of Henan province. We found a small amount of NYWM with high values in southwestern Henan province. Figure 7(b) showed the number of pixels in the number of years as wheat-maize rotation. When NYWM ranges from 1 to 5, the number of pixels in WMRA gradually increases and reaches

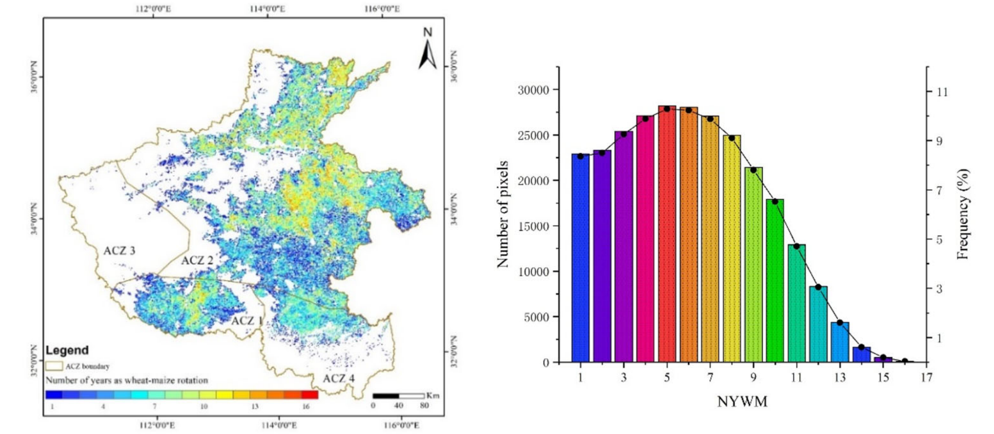

(a) (b)

Figure 7. Spatial and histogram distribution of the number of years (frequencies) as wheat-maize rotation (NYWM) during 2000–2015. (a) Distribution of NYWM; (b) number of pixels in NYWM and corresponding frequencies.

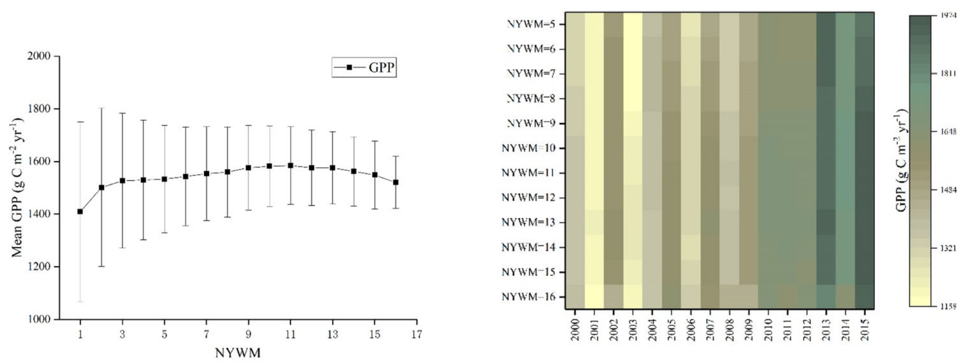

(c) (d)

Figure 8. GPP variation of non-consecutively wheat-maize rotation during 2000–2015 in Henan province, China. (a) Mean annual GPP and its standard deviation in the number of years as wheat-maize rotation. (b) Heat map of mean annual GPP in different number of years as wheat-maize rotation area (NYWM).

its peak when NYWM = 5 (with ~10.3% in corresponding frequency). Then, the number of pixels in WMRA is sharply decreased when NYWM increases from 6 to 16.

For the variation in NYWM, the mean annual GPP is increasing along with the number of years as wheat-maize rotation, and the maximum value of GPP (1584.69 g C m^{-2} $year^{-1}$) stays at NYWM = 11. The variation of mean annual GPP is relatively small, ranging from 1409.07 g C m^{-2} $year^{-1}$ at NYWM = 1 to 1584.69 g C m^{-2} $year^{-1}$ at NYWM = 11 (Figure 8(a)). Then, GPP shows decreasing trend when NYWM increases from 11 to 16. The interannual trend of standard deviation of mean annual GPP is decreased significantly, declining from 341.48 g C m^{-2} $year^{-1}$ to 99.28 g C m^{-2} $year^{-1}$. Due to great possibilities in random rotation when NYWM less than 5, only mean annual GPP in NYWM between 5–16 is demonstrated in Figure 8(b). Overall, mean annual GPP grows with the increasing of years, and the growing trend is significant from 2007 to 2015. Trends of mean annual GPP are not substantial with the growing of NYWM for a given year.

Pearson correlation coefficients (R) between number of years as wheat-maize rotation and corresponding mean annual GPP was calculated from NYWM = 1 to NYWM = 16

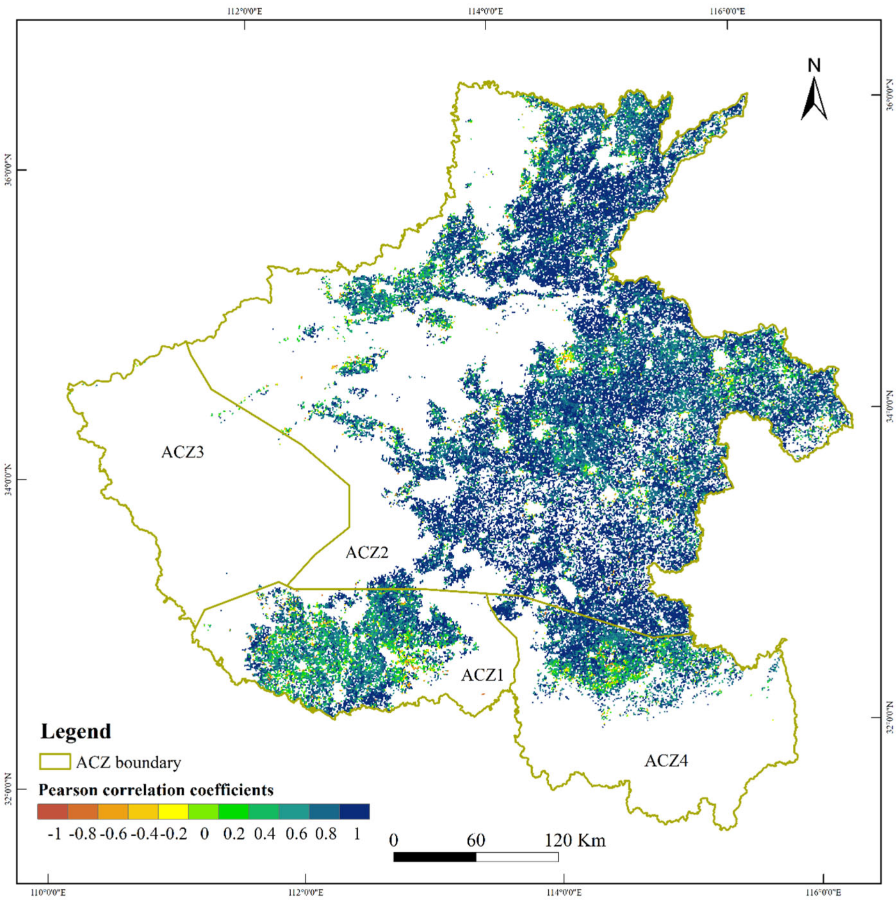

Figure 9. The spatial pattern of the Pearson correlation coefficients between annual GPP and the number of years as wheat-maize rotation area.

Table 1. Mean value of Pearson correlation coefficients (R, between number of years as wheat-maize rotation and corresponding mean annual GPP) in different number of years as wheat-maize rotation (NYWM).

NYWM	2	3	4	5	6	7	8	9	10	11	12	13	14	15	16
R value	0.60	0.62	0.66	0.66	0.67	0.68	0.69	0.71	0.72	0.73	0.73	0.72	0.73	0.73	0.70

for individual pixels (Figure 9). The mean value of Pearson correlation coefficients is 0.68 ($p < 0.01$) in Henan province, meaning high correlation between NYWM and mean annual GPP. For specific value of NYWM, R values of various cropping frequencies are greater than 0.6 and varied from 0.6 (NYWM = 2) to 0.73 (NYWM = 11, 14, 15), showing variation of R value shifted in a small range (Table 1).

4. Discussion

4.1. Main sources of error in GPP estimation of WMRA in Henan province

Annual GPP of WMRA in Henan province has grown from 25.83×10^{12} g C year^{-1} in 2000 to 64.75×10^{12} g C year^{-1} in 2015. The rise in total annual GPP while the drop in WMRA in 2002 and 2009 was mainly led by an increase of GPP in per unit area

(Figure 2). The decline in total annual GPP, while droughts mostly drove the grow in WMRA in 2001 and 2014 in the two years, which were considered the most serious droughts in the past two decades (Zhu et al. 2020). Whereas, the primary factor contributing to the decline in total annual GPP in 2003, 2006, and 2008 may be the regional low temperature and rainy in the crop growing seasons as recorded in meteorological data.

Winter wheat and summer maize rotation cropping is the most extensive type of intensified land use in Henan province (Yan et al. 2009; Wang et al. 2015). The study on regional GPP simulation in C_3–C_4 plants rotation area is of great importance to evaluate the impact of cropping practice (consecutively or non-consecutively wheat-maize rotation) on the grain production. VPM-based GPP estimates of wheat and maize agreed well with grain production in agricultural statistical data during 2000–2015. As GPP was estimated from remotely sensed imagery and ground observation data, there are a few error sources relevant to the GPP estimates. The first is the uncertainty of time–series vegetation indices extracted from spectral bands, that are often affected by many factors such as cloud and atmospheric conditions. There is much research on how to gap-fill time-series vegetation index and it has not been concluded which method is more suitable (Jin et al. 2013). The second is the ground observation data, including PAR, temperature, and the record of growing season. PAR and temperature are meteorological data derived from meteorological stations. How to interpolate site-specific meteorological data to produce meteorological raster images remains a highly debated research topic (Donat et al. 2013). The record of growing season is another type of ground observation data obtained from agricultural meteorological stations. These field-based observation data as well as phenology camera record have always been regarded as true data that used for validating the phenology derived from other indirect methods. Nevertheless, the observation data is a kind of site-based data, which need to extrapolate to a regional scale by interpolation. Alternatively, time–series vegetation index extracted from remotely sensed imagery has offered wall-to-wall information on phenology of vegetation, such as the SOS and EOS of various biomes in a given growing season (Dong et al. 2016; Wu et al. 2017). But, large discrepancies in phenology prediction for a given biome still remain due to adaptability of algorithms, diversity of species, and other factors (Wu et al. 2017; Chang et al. 2019). A reduction in the uncertainty of growing season would likely use more site-based observation (e.g. phenology camera) to provide substantial improvement in phenology prediction for croplands. The third lies in the estimation of key parameters in VPM such as the maximum LUE may varied among different regions of the same ecosystem type (Xiao et al. 2011). Usually, maximum LUE is based on analyses of half-hourly NEE and incident PAR data during peaking growing season or entire growing season at flux tower site (Baldocchi et al. 2001). Only one dominated type of land covers in most flux tower sites make it more difficult to develop maximum LUE based on a specific crop-rotation in land cover at flux tower sites. Yucheng site in Shandong, China, is a representative field station with dominated wheat-maize rotation in land cover. Previous studies have shown its key role to understand carbon exchange/balance in C_3-C_4 plants rotation area of the terrestrial biosphere (Yan et al. 2009; Bao et al. 2019). Moreover, Yucheng site is only about 110 kilometers away from the nearest county in Henan province, implying crops grow in comparable climatic conditions over the region. Therefore, we adopted the maximum LUE and other drive parameters (such as minimum, maximum and optimal temperature for photosynthetic activities) developed from the observation at Yucheng site.

The relationship between regional GPP (or NPP, biomass) and grain production was usually evaluated by the analysis of Harvest Index (HI). The $(HI)_{AGB}$ or $(HI)_{NPP}$ and grain production of different crops were often used to estimate above-ground biomass and net primary production of crops in the United States (Lobell et al. 2002; Guan et al. 2016). The empirical $(HI)_{GPP}$, $(HI)_{AGB}$ or $(HI)_{NPP}$ values vary among the crop types. Specifically, these values shift from 0.25 to 0.58 for maize, while they vary from 0.31 to 0.53 for wheat (He et al. 2018). The statistically significant relationship between annual GPP and annual grain production of wheat and maize in this study clearly demonstrates that VPM-based GPP is a feasible data source for estimating annual grain production of wheat and maize in central China.

4.2. The variation of GPP in the NYCWM

Overall, mean annual GPP grows along with the raise of NYCWM during 2000–2015 (Figure 5), showing the upward trend in fluctuation. It is highly agreed that consecutively WMARs are more likely to be managed with good water and fertilizer conditions, which could mitigate the impacts of extreme weather event (such as drought or flood) in the disaster-prone areas (Mueller et al. 2012), like WMRA in NCP. While, we noticed that the CWMRA is decreasing significantly from 2000 to 2015 (Table S1), which meant declined trend of annual total GPP in CWMRA during the 16-year periods. The substantial decrease in annual total GPP depends on several factors, such as adjustment of cropping practices in various municipalities, adaptability of crop varieties, land use/land cover change, and so on. In regard to GPP of 16-year consecutively wheat-maize rotation, the upward trend is very similar to the growing trend of GPP in CWMRA (GPP trend: 33. $77 \pm 6.57\,\mathrm{g\ C\ m^{-2}yr^{-1}}$ vs. 35. $60 \pm 6.55\,\mathrm{g\ C\ m^{-2}yr^{-1}}$), implying high consistency in GPP variation derived from changing rotation areas and fixed rotation areas in a given time period during 2000–2015.

4.3. The variation of GPP in the number of years as non-consecutively wheat-maize rotation

As showed in Figure 8a, mean interannual trend of mean annual GPP in NYWM is not significantly. Mean annual GPP has indicated a minor increase from NYWM = 1 to NYWM = 11, then it started to gradually decrease. The increase of mean annual GPP partly due to the increase in the scale of intensive production and returning farmland to forest (transform sloping farmland and desertified farmland to forest, http://www.forestry.gov.cn/tghl/2423/34042/2.html), which can be eliminate low production cropland and promote mean annual GPP. We noticed that the number of pixels in NYWM was sharply decreased from NYMW = 10. This is affected by the adjustment of agricultural planting practices (such as large-scale peanut cultivation instead of maize cropping in Zhumadian area). The alteration would affect the growing environment (fertility, temperature, humidity and so on) of WMRA. Generally, the variation of mean annual GPP was varied in a relative small range. The spatial pattern of Pearson correlation coefficients means annual GPP and NYWM have a high correlation in most WMRA. It may imply the practice of wheat-maize rotation is appropriate in most cultivated land area of Henan province.

5. Conclusions

In this study, the VPM-based GPP of winter wheat and summer maize rotation area in Henan province was estimated from MODIS imagery and meteorological data from 2000 to 2015. The results showed increasing trend of interannual GPP in a WMRA with $39.83 \pm 6.96\,\mathrm{g\ C\ m^{-2}year^{-1}}$. GPP in high values were located in the northern region and mid-east region of Henan province. For the consecutively WMRA, GPP increased along with the years as wheat-maize rotation. Furthermore, the high correlation between GPP and the number of years as wheat-maize rotation meant more frequencies in the wheat-maize rotation could obtain greater GPP. The strong linear relationship between annual GPP and annual grain production from the agricultural statistical data indicated the potential of using the VPM model to estimate annual GPP and grain production in WMRA. The research on regional GPP estimation is of great value to assess the impact of cropping rotation on grain production. The results may help our society to achieve sustainable development of WMRA in central China.

Acknowledgements

We are grateful to the Earth Observation and Modeling Facility (EOMF) from the University of Oklahoma for providing technical support of VPM model. We thank Xiaocui Wu at the University of Oklahoma for suggestion of Harvest Index calculation. H.C. gratefully acknowledges the China Scholarship Council for the financial support for a 12-month research at the University of Oklahoma.

Disclosure statement

No potential conflict of interest was reported by the authors.

Funding

This work was supported by the Key Laboratory of Aquatic Botany and Watershed Ecology, Chinese Academy of Sciences under Grant [number Y852691s01]; Science & Technology Basic Resources Investigation Program of China under Grant [number 2017FY100901], the National Science Foundation of China under Grant [number 31971491; 41701449], the project of Ministry of Ecology and Environment under Grant [number 2019HJ2096001006].

References

Allen R, Pereira L, Raes D, Smith M, Allen RG, Pereira LS, Martin S. 1998. Crop evapotranspiration: guidelines for computing crop water requirements. FAO Irrigation and Drainage Paper 56. Rome (Italy): FAO.

Angstrom A. 1924. Solar and terrestrial radiation. Report to the international commission for solar research on actinometric investigations of solar and atmospheric radiation. QJR Meteorol Soc. 50(210): 121–126.

Baldocchi D, Falge E, Gu LH, Olson R, Hollinger D, Running S, Anthoni P, Bernhofer C, Davis K, Evans R, et al. 2001. FLUXNET: a new tool to study the temporal and spatial variability of ecosystem-scale carbon dioxide, water vapor, and energy flux densities. Bull Amer Meteor Soc. 82(11):2415–2434.

Bao X, Li Z, Xie F. 2019. Environmental influences on light response parameters of net carbon exchange in two rotation croplands on the North China Plain. Sci Rep. 9(1):18702.

Bradford JB, Hicke JA, Lauenroth WK. 2005. The relative importance of light-use efficiency modifications from environmental conditions and cultivation for estimation of large-scale net primary productivity. Remote Sens Environ. 96(2):246–255.

Chang Q, Xia X, Jiao W, Wu X, Doughty R, Wang J, Du L, Zou Z, Qin Y. 2019. Assessing consistency of spring phenology of snow-covered forests as estimated by vegetation indices, gross primary production, and solar-induced chlorophyll fluorescence. Agr Forest Meteorol. 275:305–316.

Chen J, Yan H, Wang S, Gao Y, Huang M, Wang J, Xiang X. 2014. Estimation of gross primary production in Chinese terrestrial ecosystems by using VPM model. Quater Sci. 34(4):732–742.

DeFries R. 2008. Terrestrial vegetation in the coupled human-earth system: contributions of remote sensing. Annu Rev Environ Resour. 33(1):369–390.

Donat MG, Alexander LV, Yang H, Durre I, Vose R, Dunn RJH, Willett KM, Aguilar E, Brunet M, Caesar J, et al. 2013. Updated analyses of temperature and precipitation extreme indices since the beginning of the twentieth century: the HadEX2 dataset. J Geophys Res Atmos. 118(5):2098–2118.
Dong J, Xiao X, Menarguez MA, Zhang G, Qin Y, Thau D, Biradar C, Moore B, III. 2016. Mapping paddy rice planting area in northeastern Asia with Landsat 8 images, phenology-based algorithm and Google Earth Engine. Remote Sens Environ. 185:142–154.
Falge E, Baldocchi D, Olson R, Anthoni P, Aubinet M, Bernhofer C, Burba G, Ceulemans R, Clement R, Dolman H, et al. 2001. Gap filling strategies for defensible annual sums of net ecosystem exchange. Agr Forest Meteorol. 107(1):43–69.
Gallego J, Carfagna E, Baruth B. 2010. Accuracy, objectivity and efficiency of remote sensing for agricultural statistics. Hoboken (NJ): Wiley.
Goulden ML, Daube BC, Fan S-M, Sutton DJ, Bazzaz A, Munger JW, Wofsy SC. 1997. Physiological responses of a black spruce forest to weather. J Geophys Res. 102(D24):28987–28996.
Guan K, Berry JA, Zhang Y, Joiner J, Guanter L, Badgley G, Lobell DB. 2016. Improving the monitoring of crop productivity using spaceborne solar-induced fluorescence. Glob Chang Biol. 22(2):716–726.
He M, Kimball JS, Maneta MP, Maxwell BD, Moreno A, Begueria S, Wu X. 2018. Regional crop gross primary productivity and yield estimation using fused Landsat-MODIS data. Remote Sens-Basel. 10(3):372.
Huete A, Didan K, Miura T, Rodriguez EP, Gao X, Ferreira LG. 2002. Overview of the radiometric and biophysical performance of the MODIS vegetation indices. Remote Sens Environ. 83(1–2):195–213.
Huete AR, Liu HQ, Batchily K, vanLeeuwen W. 1997. A comparison of vegetation indices global set of TM images for EOS-MODIS. Remote Sens Environ. 59(3):440–451.
Hutchinson MF. 2002. Anusplin version 4.2 user guide. Canberra (Australia): Australian National University.
Jin C, Xiao X, Merbold L, Arneth A, Veenendaal E, Kutsch WL. 2013. Phenology and gross primary production of two dominant savanna woodland ecosystems in Southern Africa. Remote Sens Environ. 135:189–201.
Justice CO, Townshend JRG, Vermote EF, Masuoka E, Wolfe RE, Saleous N, Roy DP, Morisette JT. 2002. An overview of MODIS Land data processing and product status. Remote Sens Environ. 83(1–2):3–15.
Kalfas JL, Xiao X, Vanegas DX, Verma SB, Suyker AE. 2011. Modeling gross primary production of irrigated and rain-fed maize using MODIS imagery and CO2 flux tower data. Agr Forest Meteorol. 151(12):1514–1528.
Kang X, Yan L, Zhang X, Li Y, Tian D, Peng C, Wu H, Wang J, Zhong L. 2018. Modeling gross primary production of a typical coastal wetland in China using MODIS time series and CO2 eddy flux tower data. Remote Sens-Basel. 10(5):708.
Liu J, Kuang W, Zhang Z, Xu X, Qin Y, Ning J, Zhou W, Zhang S, Li R, Yan C, et al. 2014. Spatiotemporal characteristics, patterns, and causes of land-use changes in China since the late 1980s. J Geogr Sci. 24(2):195–210.
Lobell DB, Asner GP, Ortiz-Monasterio JI, Benning TL. 2003. Remote sensing of regional crop production in the Yaqui Valley, Mexico: estimates and uncertainties. Agr Ecosyst Environ. 94(2):205–220.
Lobell DB, Hicke JA, Asner GP, Field CB, Tucker CJ, Los SO. 2002. Satellite estimates of productivity and light use efficiency in United States agriculture, 1982–98. Global Change Biol. 8(8):722–735.
Luo Y, Zhang Z, Chen Y, Li Z, Tao F. 2020. ChinaCropPhen1km: a high-resolution crop phenological dataset for three staple crops in China during 2000-2015 based on leaf area index (LAI) products. Earth Syst Sci Data. 12(1):197–214.
Ma J, Zhang C, Yun W, Lv Y, Chen W, Zhu D. 2020. The temporal analysis of regional cultivated land productivity with GPP based on 2000-2018 MODIS data. Sustainability-Basel. 12(1):411.
Mc Carthy U, Uysal I, Badia-Melis R, Mercier S, O'Donnell C, Ktenioudaki A. 2018. Global food security: issues, challenges and technological solutions. Trends Food Sci Technol. 77:11–20.
Meek DW, Hatfield JL, Howell TA, Idso SB, Reginato RJ. 1984. A generalized relationship between photosynthetically active radiation and solar-radiation. Agron J. 76(6):939–945.
Monteith JL. 1977. Climate and efficiency of crop production in Britain. Philos Trans R Soc Lond B Biol Sci. 281(980):277–294.
Mueller ND, Gerber JS, Johnston M, Ray DK, Ramankutty N, Foley JA. 2012. Closing yield gaps through nutrient and water management. Nature. 490(7419):254–257.
Potter CS, Randerson JT, Field CB, Matson PA, Vitousek PM, Mooney HA, Klooster SA. 1993. Terrestrial ecosystem production: a process model-based on global satellite and surface data. Global Biogeochem Cycles. 7(4):811–841.

Raich JW, Rastetter EB, Melillo JM, Kicklighter DW, Steudler PA, Peterson BJ, Grace AL, Moore IIB, Vorosmarty CJ. 1991. Potential net primary productivity in South America: application of a global model. Ecol Appl. 1(4):399–429.
Sanchez ML, Pardo N, Perez IA, Garcia MA. 2015. GPP and maximum light use efficiency estimates using different approaches over a rotating biodiesel crop. Agr Forest Meteorol. 214–215:444–455.
Savitzky A, Golay MJE. 1964. Smoothing + differentiation of data by simplified least squares procedures. Anal Chem. 36(8):1627–1639.
Sellers PJ, Berry JA, Collatz GJ, Field CB, Hall FG. 1992. Canopy reflectance, photosynthesis, and transpiration. III. A reanalysis using improved leaf models and a new canopy integration scheme. Remote Sens Environ. 42(3):187–216.
Silva MRD, Osmar Abílio DCJ, Guimarães RF, Trancoso Gomes RA, Rosa Silva C. 2019. Wheat planted area detection from the MODIS NDVI time series classification using the nearest neighbour method calculated by the Euclidean distance and cosine similarity measures. Geocarto Int.
Spielmann FM, Wohlfahrt G, Hammerle A, Kitz F, Migliavacca M, Alberti G, Ibrom A, El-Madan TS, Gerdel K, Moreno G, et al. 2019. Gross primary productivity of four European ecosystems constrained by joint CO2 and COS flux measurements. Geophys Res Lett. 46(10):5284–5293.
Wagle P, Xiao X, Suyker AE. 2015. Estimation and analysis of gross primary production of soybean under various management practices and drought conditions. Isprs J Photogramm. 99:70–83.
Wagle P, Xiao X, Torn MS, Cook DR, Matamala R, Fischer ML, Jin C, Dong J, Biradar C. 2014. Sensitivity of vegetation indices and gross primary production of tallgrass prairie to severe drought. Remote Sens Environ. 152:1–14.
Wang Y, Hu C, Dong W, Li X, Zhang Y, Qin S, Oenema O. 2015. Carbon budget of a winter-wheat and summer-maize rotation cropland in the North China Plain. Agr Ecosyst Environ. 206:33–45.
Wu C, Peng D, Soudani K, Siebicke L, Gough CM, Arain MA, Bohrer G, Lafleur PM, Peichl M, Gonsamo A, et al. 2017. Land surface phenology derived from normalized difference vegetation index (NDVI) at global FLUXNET sites. Agr Forest Meteorol. 233:171–182.
Xiao J, Davis KJ, Urban NM, Keller K, Saliendra NZ. 2011. Upscaling carbon fluxes from towers to the regional scale: Influence of parameter variability and land cover representation on regional flux estimates. J Geophys Res. 116(G3):1–50.
Xiao X, Boles S, Frolking S, Salas W, Moore B, Li C, He L, Zhao R. 2002. Observation of flooding and rice transplanting of paddy rice fields at the site to landscape scales in China using vegetation sensor data. Int J Remote Sens. 23(15):3009–3022.
Xiao XM, Hollinger D, Aber J, Goltz M, Davidson EA, Zhang QY, Moore B. 2004. Satellite-based modeling of gross primary production in an evergreen needleleaf forest. Remote Sens Environ. 89(4):519–534.
Xiao XM, Zhang QY, Braswell B, Urbanski S, Boles S, Wofsy S, Berrien M, Ojima D. 2004. Modeling gross primary production of temperate deciduous broadleaf forest using satellite images and climate data. Remote Sens Environ. 91(2):256–270.
Xin F, Xiao X, Dong J, Zhang G, Zhang Y, Wu X, Li X, Zou Z, Ma J, Du G, et al. 2020. Large increases of paddy rice area, gross primary production, and grain production in Northeast China during 2000–2017. Sci Total Environ. 711:135183.
Xin FF, Xiao XM, Zhao B, Miyata A, Baldocchi D, Knox S, Kang M, Shim KM, Min S, Chen BQ, et al. 2017. Modeling gross primary production of paddy rice cropland through analyses of data from CO2 eddy flux tower sites and MODIS images. Remote Sens Environ. 190:42–55.
Yan H, Fu Y, Xiao X, Huang HQ, He H, Ediger L. 2009. Modeling gross primary productivity for winter wheat-maize double cropping System using MODIS time series and CO2 eddy flux tower data. Agr Ecosyst Environ. 129(4):391–400.
Zhang L, Zhang Z, Luo Y, Cao J, Tao F. 2020. Combining optical, fluorescence, thermal satellite, and environmental data to predict county-level maize yield in China using machine learning approaches. Remote Sens-Basel. 12(1):21.
Zhang Q, Lei HM, Yang DW, Xiong LH, Liu P, Fang BJ. 2020. Decadal variation in CO2 fluxes and its budget in a wheat and maize rotation cropland over the North China Plain. Biogeosciences. 17(8):2245–2262.
Zhang Y, Xiao X, Wu X, Zhou S, Zhang G, Qin Y, Dong J. 2017. Data descriptor: a global moderate resolution dataset of gross primary production of vegetation for 2000–2016. Sci Data. 4(1):170165.
Zhao MS, Heinsch FA, Nemani RR, Running SW. 2005. Improvements of the MODIS terrestrial gross and net primary production global data set. Remote Sens Environ. 95(2):164–176.
Zhu XF, Hou CY, Xu K, Liu Y. 2020. Establishment of agricultural drought loss models: a comparison of statistical methods. Ecol Indic. 112:106084.
Zuo D, Wang Y, Chen J. 1963. Characteristics of the distribution of total radiation in China. Acta Meteorologica Sinica. 1(1):78–96.